316 Vol. 40, No. 2 / February 2023 / Journal of the Optical Society of America A Research Article

Journal of the Optical Society of America A

OPTICS, IMAGE SCIENCE, AND VISION

Double-function enhancement algorithm for low-illumination images based on retinex theory

Liwei Chen,[1] Yanyan Liu,[1,*] Guoning Li,[2] Jintao Hong,[3,6] Jin Li,[4,7] and Jiantao Peng[5]

[1]Changchun University of Science and Technology, Changchun 130012, China
[2]Changchun Institute of Optics, Fine Mechanics and Physics, Chinese Academy of Sciences, Changchun 130033, China
[3]Photonics and Sensors Group, Department of Engineering, University of Cambridge, Cambridge CB3 0FA, UK
[4]School of Instrumentation and Optoelectronic Engineering, Beihang University, Beijing 100191, China
[5]Shanghai Institute of Satellite Engineering, China Aerospace Science and Technology Corporation, Shanghai 201109, China
[6]e-mail: jh2101@cam.ac.uk
[7]e-mail: jl11269@buaa.edu.cn
*Corresponding author: liuyy306@163.com

Received 9 August 2022; revised 7 December 2022; accepted 9 December 2022; posted 14 December 2022; published 17 January 2023

In order to solve the problems of noise amplification and excessive enhancement caused by low contrast and uneven illumination in the process of low-illumination image enhancement, a high-quality image enhancement algorithm is proposed in this paper. First, the total-variation model is used to obtain the smoothed V- and S-channel images, and the adaptive gamma transform is used to enhance the details of the smoothed V-channel image. Then, on this basis, the improved multi-scale retinex algorithms based on the logarithmic function and on the hyperbolic tangent function, respectively, are used to obtain different V-channel enhanced images, and the two images are fused according to the local intensity amplitude of the images. Finally, the three-dimensional gamma function is used to correct the fused image, and then adjust the image saturation. A lightness-order-error (LOE) approach is used to measure the naturalness of the enhanced image. The experimental results show that compared with other classical algorithms, the LOE value of the proposed algorithm can be reduced by 79.95% at most. Compared with other state-of-the-art algorithms, the LOE value can be reduced by 53.43% at most. Compared with some algorithms based on deep learning, the LOE value can be reduced by 52.13% at most. The algorithm proposed in this paper can effectively reduce image noise, retain image details, avoid excessive image enhancement, and obtain a better visual effect while ensuring the enhancement effect.

https://doi.org/10.1364/JOSAA.472785

1. INTRODUCTION

Image is the basis of the visual, carrying large amounts of information. It is also the foundation of computer vision tasks such as object detection and object recognition. However, the image obtained in low-illumination scenes is easily influenced by mixed noises, blurred details, and poor contrast [1], which seriously degrade the image quality and make it difficult for subsequent applications. Therefore, obtaining a higher quality of enhanced low-illumination images has become a hot topic in the field of image processing.

At present, the low-illumination image enhancement algorithms can be divided into two categories, traditional algorithms and deep learning. The traditional algorithms include mapping, histogram equalization, wavelet transform, and retinex theory. The mapping methods mainly use nonlinear functions [2–4] for global processing of low-illumination images and adjust the enhancement amplitude of different regions to avoid image distortion. Histogram equalization can achieve the enhancement effect by extending the dynamic range of the image. References [5,6] belong to the global histogram enhancement, which improve the image effect by adding brightness limits and contrast limits. In Refs. [7,8], the enhancement methods of the local histogram are adopted, and the contrast of an image is enhanced by adjusting the histogram distribution of the local area of an image by a sliding window. Wavelet transform can process both the frequency domain and the spatial domain of the image at the same time. It can take into account the detailed information of each pixel position in the low-light image. It has a unique theoretical basis and solves many problems in image processing [9,10]. Retinex theory, based on human visual characteristics, divides an image into an incident component and a reflection component [11], and removes the incident component from the original image to obtain the reflection component to achieve image enhancement. Therefore, the algorithms based on retinex theory have the characteristics of dynamic range compression and color constancy, which are conducive to enhancing details [12]. According to different path models, it can be divided into random-path-based retinex [13], multiple-iterations-based retinex [14], and center/surround-based retinex [15]. Some

representative algorithms include single-scale retinex (SSR), multi-scale retinex (MSR) [16], and multi-scale retinex with color recovery (MSRCR) [17]. In addition, the improvement of the enhancement algorithms based on retinex theory also includes another big family, namely the Milano retinex family [18], which includes random spray retinex (RSR) [19], spatio-temporal retinex-inspired envelope with stochastic sampling (STRESS) [20], Remark [21], and segmentation-based approximation of point-based sampling Milano retinex (STAR) [22]. RSR uses spray sampling instead of Brownian path, which has a better collection effect on neighboring pixel information. Therefore, in the subsequent development, light random spray retinex (LRSR) [23] and smart light random memory spray retinex (SLRMSR) [24] were proposed on the basis of RSR to reduce the computational cost. At present, related algorithms based on retinex theory are still developing, and many corresponding improved algorithms are proposed to solve the problems of image over-enhancement, color distortion, and noise amplification. In Ref. [25], the input image is decomposed based on retinex theory in a continuous sequence, and the piecewise smooth incident component and noise suppressed reflection component are estimated successively. Reference [26] proposes that the MSR algorithm is first used to enhance the Y channel in YCrCb to obtain the enhanced image; then the SSR algorithm is used to enhance the RGB image, and then the two images are weighted and fused. In the Ref. [27], according to retinex theory, image enhancement is simplified as a problem of illumination estimation. The underexposure and overexposure correction are respectively used as the trivial illumination estimation of the input image and the inverted input image to obtain two kinds of intermediate exposure correction results, and then the enhanced image is obtained by image fusion. In Ref. [28], low-rank prior is injected into the retinex decomposition process for the first time to suppress noise in the reflectivity map. In Refs. [12,29], the just-noticeable difference (JND) is used to adjust the light intensity to avoid noise amplification caused by over-enhancement, and in [29], the original image is fused with the enhanced image, and more details are preserved by using contrast limited adaptive histogram equalization (CLAHE) [30] to process the fused image. With the development of artificial intelligence, deep learning has been applied to image enhancement and achieved good results. Inspired by retinex theory, Refs. [31,32] adopt the step of decomposition first and then enhancement, and use the convolutional neural network to divide the image into an incident image and reflection image, and then combine them after training. In addition, an adjustment network is added in [32] to autonomously adjust the illumination intensity. Reference [33] proposes an enhancement method without reference, which iteratively uses the pixel value mapping curve to transform the image to obtain the enhanced image. Reference [34] regards low-light enhancement as a residual learning problem, that is, estimating the residual between low-light and normal-light images. Reference [35] constructs a dual discriminator structure to process global and local information, respectively, which can process the illumination conditions that change with the change of spatial scale.

In this paper, the traditional algorithm is used to enhance a low-illumination image, and corresponding solutions are proposed to solve the problems in image enhancement. In this paper, the total-variation (TV) model is used to denoise the V-channel image, and the adaptive gamma transform is used to enhance the details of the structure layer image obtained after denoising [36]. It successfully realizes image denoising while retaining as many image details as possible, and obtains a detailed image. Meanwhile, the hyperbolic tangent function and logarithmic function are combined to control the amplitude of image enhancement successfully and avoid image noise amplification and excessive enhancement. We also use the three-dimensional gamma function to adjust the detailed image and correct the enhanced image to achieve the restoration of image color. Finally, the saturation of the image is adjusted by an automatic threshold to obtain the final effect. The experimental results show that the algorithm successfully improves the brightness of low-illumination images, suppresses noise amplification in images, and has good performance in image fidelity and over-enhancement suppression.

2. BASIC THEORY

A. Retinex Theory

The retinex theory was put forward in the 1980s. The core idea of retinex is that an image consists of an incident component and a reflected component. The intensity of the incident component determines the dynamic range of an image pixel, while the reflected component is an inherent attribute of the object and does not change with the incident component [37]. The model is as follows:

$$I(x, y) = R(x, y) \cdot L(x, y), \tag{1}$$

where $I(x, y)$ is the observation image, $R(x, y)$ is the reflection component, and $L(x, y)$ is the incident component. It is usually converted to a logarithmic form to reduce computational complexity:

$$\log R(x, y) = \log I(x, y) - \log L(x, y). \tag{2}$$

Based on this theory, a classical SSR algorithm was proposed. A Gaussian kernel function is convolved with the original image to estimate the incident component, and the reflection component is obtained by using Eq. (3) to realize the enhancement of low-illumination images. The formula is as follows:

$$\log R_i(x, y) = \log I_i(x, y) - \log(I_i(x, y) \otimes G(x, y)), \tag{3}$$

where R_i represents the reflective components of different color channels, $\otimes$ is the convolution symbol, G is the Gaussian kernel function, and its formula is

$$G(x, y) = \frac{1}{2\pi\sigma^2} \exp\left(-\frac{x^2 + y^2}{2\sigma^2}\right), \tag{4}$$

where σ is the standard deviation of the Gaussian function. When it is small, the enhanced image retains more details, but it is easy to cause color distortion in an image. When it is large, the enhanced image keeps a good color, but the image becomes blurred [38], and the halo effect easily occurs in the brighter area.

In order to solve the above problems, an MSR algorithm was proposed to enhance low-illuminance image at different scales, and its expression is as follows:

$$\log R_i(x, y) = \sum_{j}^{N} \omega_j \left\{ \log I_i(x, y) - \log(I_i(x, y) \otimes G_j(x, y)) \right\}, \tag{5}$$

where N is 3, representing the three scales, ω_j represents the first j scale parameter, and, in general, $\omega_1 = \omega_2 = \omega_3 = 1/3$, G_j represents the corresponding Gaussian kernel function with different σ.

B. Guided Filtering

Guided filtering is an adaptive local linear filter, which has good edge preserving characteristics and can preserve the edge details of the image while smoothing the image. Its expression is as follows [39,40]:

$$q(x, y) = \frac{1}{|w|} \sum_{k(x,y) \in M_k} [a_k J(x, y) + b_k], \tag{6}$$

where, $q(x, y)$ is the output image, $J(x, y)$ is the guidance image, M_k is the filtering window with radius r, $|w|$ is the total number of pixels in window M_k, $k(x, y)$ is the pixel value in window M_k, k is the center of the filtering window, a_k and b_k are the linear coefficients when the center of the filtering window is located at pixel $k(x, y)$, and their expressions are, respectively, as follows:

$$a_k = \frac{\frac{1}{|w|} \sum_{k(x,y) \in M_k} J(x, y) p(x, y) - u_k \overline{p_k}}{\sigma_k^2 + \varepsilon}, \tag{7}$$

$$b_k = \overline{p_k} - a_k u_k, \tag{8}$$

where $p(x, y)$ represents the input image, σ_k represents the variance of the guidance image $J(x, y)$ in window M_k, $\overline{p_k}$ represents the average value of image $p(x, y)$ corresponding to filtering window M_k, u_k represents the mean value of image $J(x, y)$ corresponding to filtering window M_k, and ε represents a regularization parameter.

3. METHOD

To obtain high-quality enhancement performance without noise amplification in the low-illumination condition, we present an efficient algorithm based on retinex theory. The overall framework of the image enhancement algorithm is shown in Fig. 1. The proposed algorithm is composed of a TV denoising unit, an adaptive saturation adjustment unit, a double-function image fusion enhancement unit, and a three-dimensional gamma correction unit. The original image is the input RGB format image, which is first converted to HSV format, and then the optimized S-channel and V-channel images, namely S' and I_{img}, are obtained through different processing methods. Finally, the three channel images obtained are reconstituted into HSV format and then converted into RGB format. The V-channel image needs to be smoothed by the TV model to get the image I_u^V, and then the details are enhanced by adaptive gamma enhancement to get the image I_d. The S-channel image only needs to be smoothed to get the image I_u^S. The following sections will discuss the details of each unit for this algorithm.

A. TV Denoising

According to retinex theory, after removing the incident component in the image, the reflected component obtained can show the true color of the object, so the related algorithms based on retinex theory have good color retention ability. However, in practice, it is difficult to accurately estimate the incident component in the image, which may lead to defects in the obtained

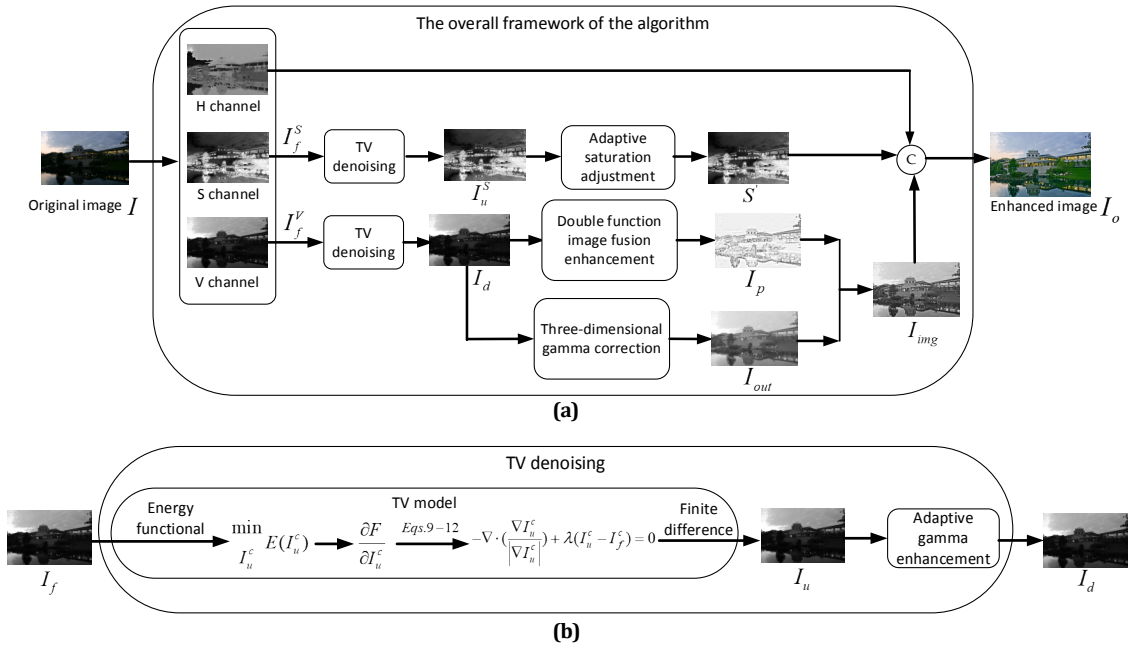

Fig. 1. (a) Overall framework of the algorithm. (b) Framework of TV denoising.

reflection component, destroy the correlation between different color channels, and lead to color distortion in the image enhancement result [38,41]. To avoid this situation, the image can be transferred to a HSV color model. Through the analysis of the conversion process, it is found that the transformed image noise is mainly concentrated in the S and V channels [42]. Therefore, to reduce the noise amplification in the image enhancement process, the above image channels need to be denoised first.

Among the denoising methods based on partial differential equations, a TV model has been proved to be one of the most effective algorithms [43,44]. Through this model, the image denoising problem can be transformed into an unconstrained optimization problem to solve the minimum energy functional, and the expression is shown as follows:

$$\min_{I_u^c} E(I_u^c) = \min_{I_u^c} \iint_\Omega |\nabla I_u^c| \mathrm{d}x\mathrm{d}y + \frac{\lambda}{2}\iint_\Omega (I_u^c - I_f^c)^2 \mathrm{d}x\mathrm{d}y, \tag{9}$$

where c represents the different channels, namely the S channel or V channel, I_u^c represents the ideal image of the channel, and I_f^c represents the observed image of the channel. In Eq. (9), the former is a regularization term and $\nabla = \left(\frac{\partial}{\partial x}, \frac{\partial}{\partial y}\right)$ represents a Hamiltonian operator, $|\nabla I_u^c| = \sqrt{{I_{u_x}^c}^2 + {I_{u_y}^c}^2}$; this term can suppress noise and play a smoothing role on the image. The latter term is the fidelity term, which is used to keep the edge information of the image, so that the image is closer to the original image. The λ represents the regularization parameter, which is used to balance the regularization term and the fidelity term, Experiments show that better results can be achieved when the value is 90. The following function can be obtained from Eq. (9):

$$F = \frac{\lambda}{2}(I_u^c - I_f^c)^2 + |\nabla I_u^c| = \frac{\lambda}{2}(I_u^c - I_f^c)^2 + \sqrt{I_{ux}^{c2} + I_{uy}^{c2}}. \tag{10}$$

When the minimum value is obtained through Eq. (9), Eq. (10) satisfies the Euler Lagrange equation, and the formula is as follows:

$$\frac{\partial F}{\partial I_u^c} = \frac{\partial}{\partial x}\left(\frac{\partial F}{\partial I_{u_x}^c}\right) + \frac{\partial}{\partial y}\left(\frac{\partial F}{\partial I_{u_y}^c}\right). \tag{11}$$

The calculation expression of the divergence is given as follows:

$$\mathrm{div}F = \nabla \cdot F = \frac{\partial F_x}{\partial x} + \frac{\partial F_y}{\partial y}. \tag{12}$$

By combining Eqs. (9)–(12), the final Euler Lagrange equation can be obtained, which is expressed as follows:

$$-\nabla \cdot \left(\frac{\nabla I_u^c}{|\nabla I_u^c|}\right) + \lambda(I_u^c - I_f^c) = 0, \tag{13}$$

where $1/|\nabla I_u^c|$ represents the diffusion coefficient. $|\nabla I_u^c|$ is large at the edge of the image, and the diffusion coefficient is small so that the edge can be preserved. On the contrary, $|\nabla I_u^c|$ is small in the smooth area of the image, the diffusion coefficient is large, and the noise can be removed [45]. The finite difference method is used to solve the above equation and get a smooth image I_u^c; the formula is as follows [46]:

$$I_{u(i,j)}^{c(n+1)} = I_{u(i,j)}^{c(n)} - \Delta t\lambda(I_{u(i,j)}^{c(n)} - I_{f(i,j)}^{c}) + \Delta t\left(\nabla \cdot \left(\frac{\nabla I_{u(i,j)}^{c(n)}}{\left|\nabla I_{u(i,j)}^{c(n)}\right|}\right)\right), \tag{14}$$

where n represents the number of iterations, and t represents the time step. Experiments show that better results can be achieved when the two are 100 and 0.25, respectively.

Although most of the image information is retained in the denoising process, part of the image details are also lost. So, the image details need to be improved [36]. In Ref. [47], the gray information and variance of the image are used to set the gamma transform parameters to highlight the details of the image. The formula is as follows:

$$I_d = I_u^V(x,y)^{\left(\frac{N(x,y)}{I_u^V(x,y)} + b(x,y)\right)}, \tag{15}$$

$$N(x,y) = \frac{\sum_{m,n} I_u^V(x,y)}{m \cdot n}, \tag{16}$$

$$b(x,y) = \frac{\sum_{m,n} \left(I_u^V(x,y) - N(x,y)\right)^2}{m \cdot n}, \tag{17}$$

where N and b are the average gray value and variance of the local area of the pixel point centered on $I_u^V(x,\ y)$.

Based on Eqs. (9)–(17), the denoising effect of the images is shown in Fig. 2. By observing the images in Fig. 2, it can be found that the denoising effect of the denoised image is significantly improved compared with the original image. The noise points in the image background are effectively eliminated, and the main structural layer of the image is effectively preserved. However, the edge effect of the image also becomes blurred to a certain extent, which reduces the hierarchical sense of the image and affects the subsequent enhancement effect of the image. After further processing with the adaptive gamma transform, it can be found from the detailed image that the edge details of objects and some tiny traces in the image are expanded, enriching the sense of image layers, and improving the contrast.

(a) (b) (c)

Fig. 2. Processed image: (a) original image. (b) Denoised image. (c) Detailed image.

B. Double-Function Image Enhancement

As mentioned above, the traditional MSR algorithm uses the Gaussian kernel function that emphasizes spatial information to estimate the incident image and ignores the edge information of the image, which leads to the occurrence of a halo in the enhanced image at the light source. This problem can be effectively solved by using guided filtering that considers both to estimate the incident image. The initial adjustment image I_d is used as the input image and the guidance image. The incident component of the image is obtained by combining Eqs. (6)–(8), and then the preliminary image enhancement result I_l is obtained by Eq. (5).

In the MSR algorithm, logarithmic image data is obtained according to Eq. (5). In order to avoid a negative infinity state, a smaller parameter is usually added, namely $\log(x + \text{eps})$. It leads to the error of some data. In addition, in some areas, the estimated pixel value is much smaller than itself and the reflected image data is too large, which leads to the phenomenon of excessive enhancement of images after inverse logarithm processing. Therefore, the continuity and finiteness of the hyperbolic tangent function are used to compensate for partial data and suppress excessive image enhancement [48]. However, the hyperbolic tangent function cannot be directly used to enhance the image, and its effect image is shown in Fig. 3.

As shown in Fig. 3, the maximum value of the hyperbolic tangent function approaches 1. Although the enhancement of the dark region can be realized and excessive enhancement of the bright region can be inhibited, the enhancement effect between the two degrees is not obvious; the enhancement effect of the whole image is dim, while the logarithmic function changes greatly after inverse transformation. Therefore, this paper utilizes the characteristics of both. The fusion parameters are designed according to the brightness of the image local region to achieve a balance between the two images. The formula is shown below:

$$I_p = \alpha I_l + \beta I_t, \tag{18}$$

$$\alpha = \frac{\sum_{m,n} I_t}{\sum_{m,n} I_l}, \tag{19}$$

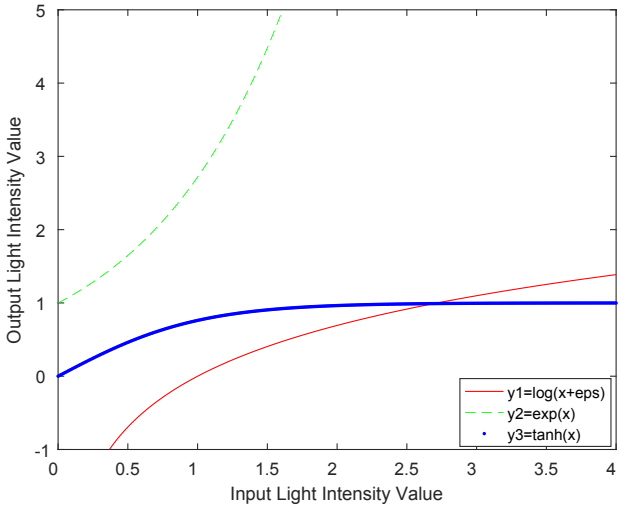

Fig. 3. Function contrast image.

$$I_t = \sum_j^N \omega_j \left\{ \tanh\left(\frac{I_d(x,y)}{I_d(x,y) \otimes G_j(x,y)} \right) \right\}, \tag{20}$$

where α and β are the adjusting parameters, $\alpha + \beta = 1$. I_l and I_t are enhanced by a logarithmic function and hyperbolic tangent function, respectively. In the above formula, *tanh* is the hyperbolic tangent function, and its expression is as follows:

$$\tanh(x) = \frac{\exp(x) - \exp(-x)}{\exp(x) + \exp(-x)}. \tag{21}$$

Using Eqs. (18)–(21), an image effect example is shown in Fig. 4. The image obtained by logarithmic function has higher overall brightness, and more loss of local details, and a halo appears at the edge of some buildings, while the image obtained by the hyperbolic tangent function has lower overall brightness, low contrast, and a blurred image. The image obtained by combining the two functions can suppress excessive enhancement and the edge halo, but the "white fog" caused by the darkest region of the image after enhancement has not been solved, and it still needs to be further processed.

C. Three-Dimensional Gamma Correction

In order to solve the above "white fog" problem, this section uses gamma transform to adjust the detailed image and then, on this basis, correct the enhanced image. Considering the brightness and detail information of the image, the gamma parameter values are set from three dimensions, namely the gray scale, variance, and gradient values of the image. The formula is as follows:

$$I_{\text{out}} = I_d^{(\psi \cdot \exp(A) + \mu \cdot \exp(B) + \nu \cdot \exp(C))}, \tag{22}$$

where ψ, μ, and ν are the control parameters, which are 0.1, 0.1, and 0.05 after the test, respectively; A is the gray level information of the image, which is the ratio between the pixel value of input image $I_d(x, y)$ and the maximum pixel value in the $m \times n$ region of the image; B is the local mean gradient in a region $m \times n$ centered on $I_d(x, y)$, as shown in formula

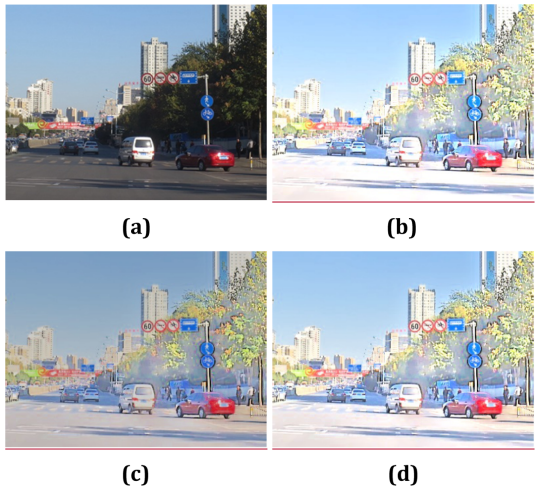

Fig. 4. Images of different functions: (a) original image, (b) logarithmic image, (c) hyperbolic tangent image, and (d) double-function image.

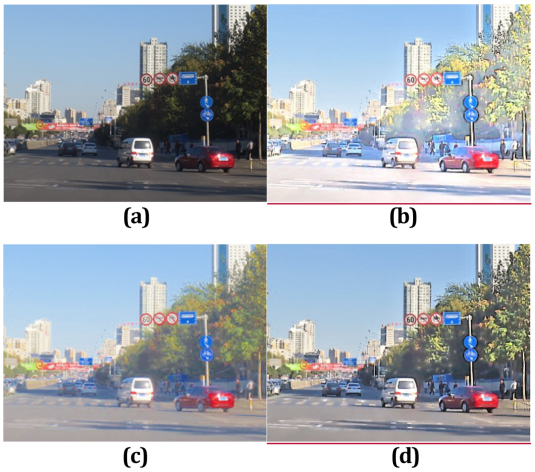

Fig. 5. Image correction: (a) original image, (b) uncorrected image, (c) gamma corrected image, and (d) three-dimensional corrected image.

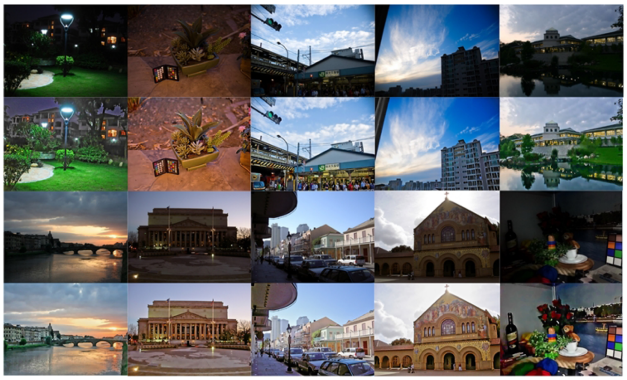

Fig. 6. Effect image of algorithm.

Eq. (23); and C is the local variance of the image, which can be obtained by referring to formula Eq. (17). The final image I_{img} is

$$B(x, y) = \frac{\sum_{m,n} |\nabla I_d(x, y)|}{m \cdot n}, \tag{23}$$

$$I_{\text{img}} = I_p \cdot I_{\text{out}}. \tag{24}$$

Based on Eqs. (22)–(24), the correction effect of an image is shown in Fig. 5. As shown in Fig. 5, the contrast of the corrected image is significantly improved, the sense of layers of the image is richer, and the overall brightness of the image is coordinated. Compared with the original image, the enhancement of the highlighted areas, such as the sky and buildings, is inhibited, while the enhancement effect of the low-illumination areas, such as trees, pedestrians, and roads, is obvious.

D. Saturation Regulation

In low-illuminance image, the image saturation in the dark area is low. Directly transforming the processed channel images into an RGB image will lead to the phenomenon of a "dark spot" in the dark area of the image. This phenomenon can be alleviated by adjusting the saturation channel of the image, and the formula is shown as follows:

$$S' = \begin{cases} 1 + 0.8 \cdot \log\left(\frac{S_m}{I_u^S(i,j)+0.5\cdot S_g(i,j)}\right), & I_u^S(i, j) \le \vartheta \\ \exp\left(\frac{S_m - I_u^S(i,j)}{2}\right), & \text{else,} \end{cases} \tag{25}$$

where S_m is the mean value in a region $m \times n$ centered on this point, S_g is the gradient of this point, and ϑ is the sum of the global mean value of the S channel and the gradient value of this point.

4. EXPERIMENTAL RESULTS

In order to prove the effectiveness of the algorithm, we selected several groups of images for experiment. These images are derived from the datasets presented in Refs. [8,49,50]. The specific implementation effects of the algorithm are shown in Fig. 6.

In order to further prove the superiority of the algorithm, we chose some enhanced images to compare with the enhanced images of other algorithms from both subjective and objective aspects.

A. Subjective Evaluation

To verify the effectiveness of the algorithm, we selected some images for the enhancement experiments; the image size is 640 × 480, compared with the MSRCR [17], low-light image enhancement via illumination map estimation (LIME) [49], CLAHE [30], the low-rank regularized retinex model (LR3M) [28], Retinex-Net [31], the deep lighten network (DLN) [34], joint enhancement and denoising (JED) [25], and dual illumination estimation for robust exposure correction (DIEREC) [27]. In our experiments, the radius r of the filtering window is 15, and the three regularization parameters ε are 0.005, 0.015, and 0.025, respectively.

The observation results are shown in Figs. 7–11. From Figs. 7(b)–11(b), we find that the overall visual effect of images enhanced by the MSRCR algorithm is white, with serious color loss and low image contrast. From Figs. 7(c)–11(c) we find that the contrast and color retention of the images obtained by the LIME algorithm are relatively high, but also maintain a certain enhancement amplitude in the bright area of the image, resulting in an excessive enhancement in this area and image noise amplification. From Figs. 7(d)–11(d), it can be found that the texture details of the enhanced images obtained by the CLAHE algorithm are seriously lost, and there is a phenomenon of color distortion in the sky region of the enhancement images. It can be seen from Figs. 7(e)–11(e) that the image effect obtained by using the LR3M algorithm is slightly blurred. In Fig. 7(e), there is excessive enhancement and a virtual shadow at the light source. From Figs. 7(f)–11(f), it can be seen that there is noise amplification and detail loss in the enhanced images obtained with Retinex-Net. For DLN enhanced images from Figs. 7(g)–11(g), the images have a good enhancement effect in the lower brightness area, but there is a general phenomenon of over-enhancement in the brighter area. From Figs. 7(h)–11(h), we find that the enhanced images obtained by the JED algorithm have good overall vision, but the image details are also

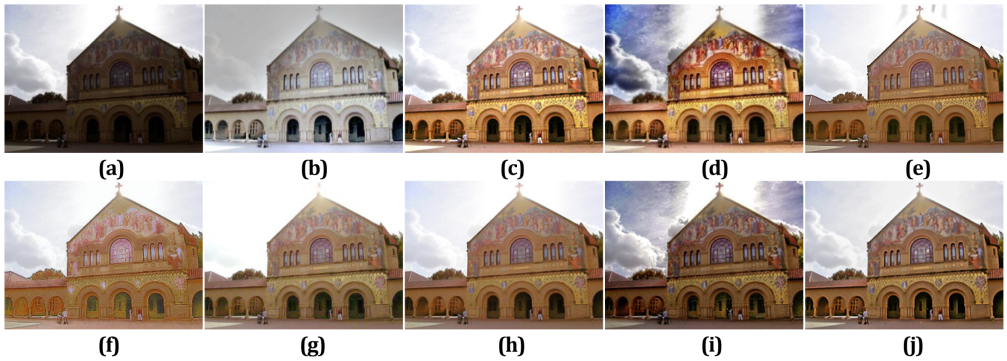

Fig. 7. (a) Original. (b) MSRCR. (c) LIME. (d) CLAHE. (e) LR3M. (f) Retinex-Net. (g) DLN. (h) JED. (i) DIEREC. (j) Proposed.

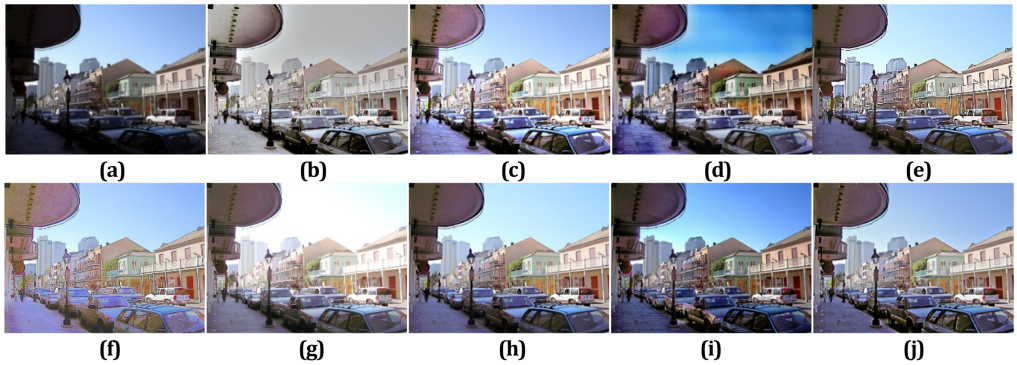

Fig. 8. (a) Original. (b) MSRCR. (c) LIME. (d) CLAHE. (e) LR3M. (f) Retinex-Net. (g) DLN. (h) JED. (i) DIEREC. (j) Proposed.

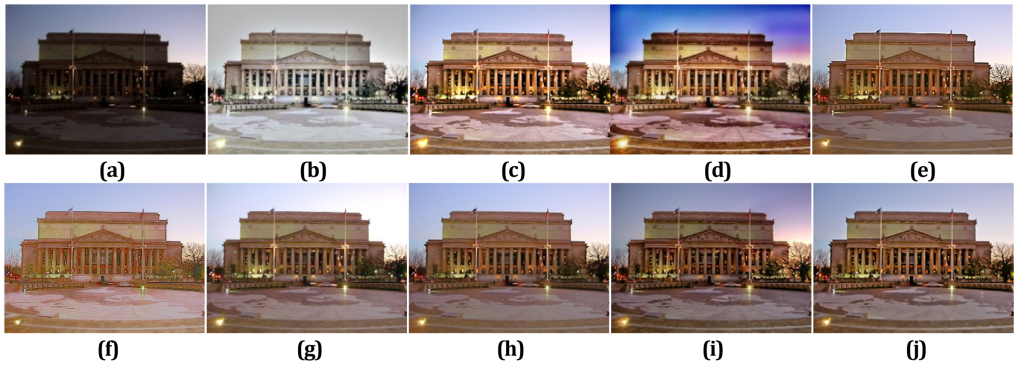

Fig. 9. (a) Original. (b) MSRCR. (c) LIME. (d) CLAHE. (e) LR3M. (f) Retinex-Net. (g) DLN. (h) JED. (i) DIEREC. (j) Proposed.

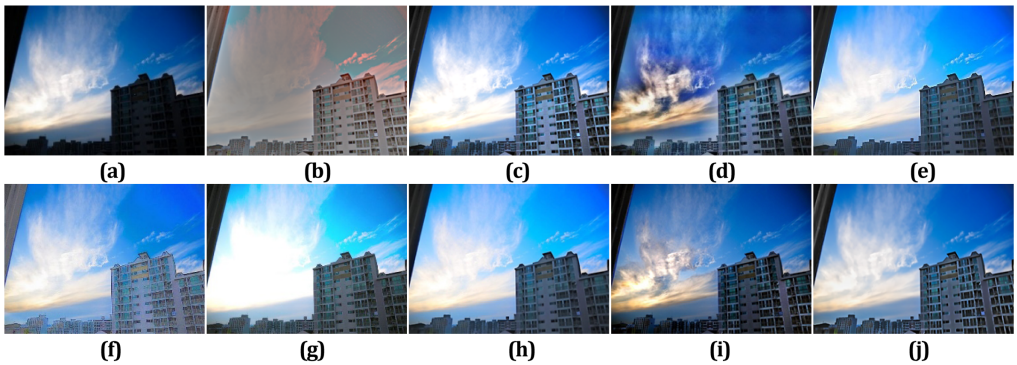

Fig. 10. (a) Original. (b) MSRCR. (c) LIME. (d) CLAHE. (e) LR3M. (f) Retinex-Net. (g) DLN. (h) JED. (i) DIEREC. (j) Proposed.

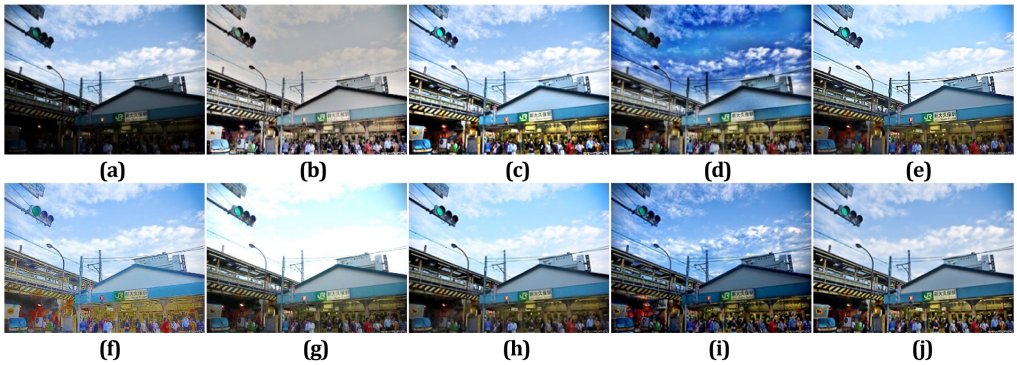

Fig. 11. (a) Original. (b) MSRCR. (c) LIME. (d) CLAHE. (e) LR3M. (f) Retinex-Net. (g) DLN. (h) JED. (i) DIEREC. (j) Proposed.

slightly blurred, which is the same as LR3M. From Figs. 7(i)–11(i), it can be found that the enhanced images obtained by the DIEREC algorithm have insufficient enhancement in the local area of the image, as shown in Fig. 10(i), and some images are distorted, as shown in Figs. 7(i). Figures 7(j)–11(j) are the proposed algorithms in this paper. Compared with other algorithms, the images are preprocessed, so the image noise is effectively suppressed and the details of the image are also preserved. The proposed algorithm in this paper can not only realize the enhancement effect but also effectively suppress the phenomenon of excessive enhancement in the bright area of the images; for example, the sky and light source areas in each scene have better visual effects.

B. Objective Evaluation

The peak signal-to-noise ratio (PSNR) is used to measure the noise of the enhanced image, and structural similarity (SSIM) is used to measure the structural similarity between the enhanced image and the original image to judge the distortion of the image. Standard deviation (SD) is used to reflect the dispersion degree of pixels relative to the mean to characterize the image contrast. The information entropy (IE) is used to reflect the richness of image information and characterize the complexity of image. The lightness order error (LOE) [50] is used to measure the preservation of the naturalness of the enhanced image. In the experimental results obtained, the higher the values of PSNR, SSIM, SD, and IE obtained, the better the image effect. On the contrary, the lower the LOE value, the better the image effect. We show the optimal and suboptimal results for each experiment in bold italic and bold, respectively. The specific parameters of various algorithms are shown in Tables 1–5.

As shown in Table 1, the PSNR of the images obtained by the proposed algorithm is second only to the DIEREC algorithm, and it is improved in different degrees compared with other algorithms. Compared with MSRCR, LIME, CLAHE, LR3M, and JED, the PSNR has improved by 58.46%, 36.87%, 24.64%, 6.06%, and 5.09%, respectively, and compared with the Retinex-Net and DLN, the PSNR has improved by 31.87% and 41.06%, effectively reducing the image noise. In Table 2, the SSIM of the algorithm in this paper is second only to the DIEREC algorithm. Compared with the LR3M algorithm and JED algorithm, the SSIM of the proposed algorithm is improved by about 6.10% and 3.19%, respectively, which avoids the huge distortion of the image compared with the original image. In Table 3, the SD value of the algorithm in this paper is slightly smaller than the LIME, but from the perspective of the image effect, the proposed algorithm still has a good ability to maintain details. In Table 4, the IE of this algorithm is second only to the CLAHE algorithm and higher than other algorithms. Compared with the DLN algorithm, the improvement is the highest, which is about 18.02%. In Table 5, the LOE of the algorithm presented in this paper is the lowest. Compared with other algorithms, the effect of this algorithm is greatly improved. Compared with the MSRSR, LIME, CLAHE, LR3M, JED, and DIEREC algorithms, the maximum reduction can be 79.95%, and compared with the Retinex-Net and DLN algorithms, the reduction is 52.13% and 19.08%, respectively, which have great advantages. Combining the subjective and objective aspects of the image, the algorithm in this paper has better overall performance and has certain advantages over other algorithms.

Table 1. Comparison of Image PSNR

Image	MSRCR	LIME	CLAHE	LR3M	Retinex-Net	DLN	JED	DIEREC	Proposed
Fig. 7	8.0750	10.2291	9.7745	13.3078	11.5351	12.2034	13.7423	***15.9812***	**14.0252**
Fig. 8	10.2918	10.1171	13.1106	13.9916	10.4461	10.5819	14.0420	***17.5930***	**14.1186**
Fig. 9	7.2332	8.9235	10.2332	12.4189	9.6542	11.0284	12.6383	***14.8569***	**12.9890**
Fig. 10	8.9312	12.7726	13.3584	13.2545	11.2153	10.8836	12.7390	***18.8025***	**15.7365**
Fig. 11	11.0291	10.7060	11.4494	15.0996	11.8980	12.4837	**15.5393**	***17.2493***	15.3276
Mean	9.1121	10.5497	11.5852	13.6145	10.9497	10.2362	13.7402	***16.8966***	**14.4394**

Table 2. Comparison of Image SSIM

Image	MSRCR	LIME	CLAHE	LR3M	Retinex-Net	DLN	JED	DIEREC	Proposed
Fig. 7	0.4773	0.5505	0.4080	0.5935	0.5615	0.5600	0.6177	***0.6394***	**0.6388**
Fig. 8	0.4006	0.5939	0.5922	0.6321	0.5885	0.3856	0.6512	***0.7207***	**0.6703**
Fig. 9	0.2968	0.4489	0.3512	0.5420	0.4620	0.4953	0.5637	***0.6095***	**0.5772**
Fig. 10	0.2302	0.6694	0.5981	0.6591	0.6275	0.5499	0.6529	***0.7445***	**0.7146**
Fig. 11	0.2737	0.6518	0.5387	0.6878	0.6352	0.4198	***0.7171***	0.6899	**0.7035**
Mean	0.3357	0.5829	0.4976	0.6229	0.5749	0.4821	0.6405	***0.6808***	**0.6609**

Table 3. Comparison of Image SD

Image	MSRCR	LIME	CLAHE	LR3M	Retinex-Net	DLN	JED	DIEREC	Proposed
Fig. 7	0.1978	0.2751	0.2460	0.2797	0.2389	***0.2920***	**0.2844**	0.2635	0.2777
Fig. 8	0.2378	0.2620	0.2364	**0.2881**	0.1921	***0.2954***	0.2839	0.2531	0.2478
Fig. 9	0.2091	**0.2380**	0.2014	0.2174	0.1749	***0.2665***	0.2241	0.1892	0.2116
Fig. 10	0.2195	**0.2778**	0.1915	0.2695	0.2049	***0.2987***	0.2689	0.2346	0.2556
Fig. 11	0.2605	0.3016	0.2116	0.3166	0.2315	***0.3385***	**0.3241**	0.2676	0.2844
Mean	0.2250	0.2709	0.2174	0.2743	0.2085	***0.2982***	**0.2771**	0.2416	0.2554

Table 4. Comparison of Image IE

Image	MSRCR	LIME	CLAHE	LR3M	Retinex-Net	DLN	JED	DIEREC	Proposed
Fig. 7	7.2070	7.3703	***7.8465***	7.5569	7.6575	6.0262	7.4770	**7.7344**	7.6929
Fig. 8	7.3586	7.4271	***7.9426***	7.6325	7.4984	6.7205	7.6985	7.6931	**7.8353**
Fig. 9	7.2808	7.8193	***7.8905***	**7.8207**	7.6683	7.4378	7.7907	7.6513	7.7969
Fig. 10	6.8935	7.6407	***7.8727***	7.5205	7.6375	6.6456	7.4826	7.7094	**7.8114**
Fig. 11	7.1932	7.4093	***7.9372***	7.4737	7.6813	6.1471	7.4563	7.7830	**7.7847**
Mean	7.1866	7.5333	***7.8979***	7.6001	7.6286	6.5954	7.5810	7.7142	**7.7842**

Table 5. Comparison of Image LOE

Image	MSRCR	LIME	CLAHE	LR3M	Retinex-Net	DLN	JED	DIEREC	Proposed
Fig. 7	986.4367	301.6633	900.2940	229.1155	340.6755	235.9075	***167.0367***	257.0033	**220.0170**
Fig. 8	958.1582	263.4301	406.8269	261.9773	448.2594	***147.8415***	226.3490	223.4806	**184.5203**
Fig. 9	799.4448	271.8690	613.3749	244.1949	427.1367	***126.9063***	**205.8839**	331.1307	249.8173
Fig. 10	942.2824	**261.4358**	753.5755	976.6908	550.1650	344.6213	996.1461	399.2855	***134.4097***
Fig. 11	1373.9960	336.1939	505.1650	466.6208	353.5218	398.6355	498.1139	**278.9129**	***225.9137***
Mean	1012.0636	286.9184	635.8472	435.7198	423.9517	**250.7824**	418.7059	297.9626	***202.9356***

5. CONCLUSION

This paper proposed an efficient image enhancement algorithm capable of overcoming the problems of noise amplification and excessive enhancement in the process of low-illumination image enhancement. This work adopts a TV denoising method to preprocess image, and the adaptive gamma transform is used to enhance the image details. The *tanh* function and logarithm function are combined to obtain the preliminary enhanced image to avoid excessive image enhancement. Meanwhile, a three-dimensional gamma transform is used to adjust and correct the enhanced image. From the subjective result, it is found that the enhanced image achieves the denoising effect and retains details effectively, and avoids excessive image enhancement on the basis of ensuring the enhancement effect. From the objective results, compared with the MSRCR, LIME, CLAHE, LR3M, JED, and DIEREC algorithms, the LOE value of the proposed algorithm can be reduced by up to 79.95%, 29.27%, 68.08%, 53.43%, 51.53%, and 31.89%, respectively. Compared with the Retinex-Net and DLN algorithms, the reduction is 52.13% and 19.08%, respectively. The enhanced image maintains better naturalness and has certain advantages in other parameters.

Funding. Innovation Foundation of Changchun University of Science and Technology (XJJLG-2018-07); Education Department of Jilin Province, China (JJKH20210838KJ).

Acknowledgment. Yanyan Liu thanks the Innovation Foundation of Changchun University of Science and Technology and the Education Department of Jilin Province, China.

Disclosures. The authors declare no conflicts of interest.

Data availability. The data that support the findings of this study are available from the corresponding author upon reasonable request.

REFERENCES

1. X. Jiang and H. Yao, "Summary of nighttime image enhancement methods," Intell. Comput. Appl. **10**, 394–403 (2020).
2. E. Peli, "Contrast in complex images," J. Opt. Soc. Am. A **7**, 2032–2040 (1990).
3. R. C. Gonzalez, *Digital Image Processing* (Pearson Education India, 2009).

4. X. Yang, X. Jiang, and J. Du, "Low illumination image enhancement algorithm based on gamma transformation and fractional order," Comput. Eng. Des. **42**, 762–769 (2021).
5. A. M. Reza, "Realization of the contrast limited adaptive histogram equalization (CLAHE) for real-time image enhancement," J. VLSI Signal Process. Syst. Signal Image Video Technol. **38**, 35–44 (2004).
6. H. Ibrahim and N. S. P. Kong, "Brightness preserving dynamic histogram equalization for image contrast enhancement," IEEE Trans. Consum. Electron. **53**, 1752–1758 (2007).
7. J. A. Stark, "Adaptive image contrast enhancement using generalizations of histogram equalization," IEEE Trans. Image Process. **9**, 889–896 (2000).
8. C. Lee, C. Lee, and C. S. Kim, "Contrast enhancement based on layered difference representation of 2D histograms," IEEE Trans. Image Process. **22**, 5372–5384 (2013).
9. Q. Li and Q. Liu, "Adaptive enhancement algorithm for low illumination images based on wavelet transform," Chin. J. Lasers **42**, 280–286 (2015).
10. G. Wang, Z. Shi, W. Tan, S. Li, and T. Gao, "Image enhancement algorithm for fusion of double-density dual-tree complex wavelet transform and multi-scale retinex," Comput. Dig. Eng. **45**, 870–873 (2017).
11. E. H. Land and J. J. McCann, "Lightness and retinex theory," J. Opt. Soc. Am. **61**, 1–11 (1971).
12. Q. Fu, C. Jung, and K. Xu, "Retinex-based perceptual contrast enhancement in images using luminance adaptation," IEEE Access **6**, 61277–61286 (2018).
13. E. Provenzi, C. L. De, A. Rizzi, and D. Marini, "Mathematical definition and analysis of the Retinex algorithm," J. Opt. Soc. Am. A **22**, 2613–2621 (2005).
14. D. G. Hwang, W. R. Lee, Y. J. Oh, and B. M. Jun, "Frankle-McCann Retinex by shuffling," in *International Conference on Hybrid Information Technology* (Springer, 2012). pp. 381–388.
15. A. S. Parihar and K. Singh, "A study on Retinex based method for image enhancement," in *2nd International Conference on Inventive Systems and Control (ICISC)* (IEEE, 2018), pp. 619–624.
16. D. J. Jobson, Z. Rahman, and G. A. Woodell, "Properties and performance of a center/surround Retinex," IEEE Trans. Image Process. **6**, 451–462 (1997).
17. D. J. Jobson, Z.-U. Rahman, and G. A. Woodell, "A multiscale retinex for bridging the gap between color images and the human observation of scenes," IEEE Trans. Image Process. **6**, 965–976 (1997).
18. A. Rizzi and C. Bonanomi, "Milano Retinex family," J. Electron. Imaging **26**, 031207 (2017).
19. E. Provenzi, M. Fierro, A. Rizzi, L. D. Carli, D. Gadia, and D. Marini, "Random spray Retinex: a new Retinex implementation to investigate the local properties of the model," IEEE Trans. Image Process. **16**, 162–171 (2007).
20. O. Kolas, I. Farup, and A. Rizzi, "Spatio-temporal Retinex-inspired envelope with stochastic sampling: a framework for spatial color algorithms," J. Imaging Sci. Technol. **55**, 40503-1 (2011).
21. G. Gianini, A. Rizzi, and E. Damiani, "A Retinex model based on absorbing Markov chains," Inf. Sci. **327**, 149–174 (2016).
22. M. Lecca, "STAR: a segmentation-based approximation of point-based sampling Milano Retinex for color image enhancement," IEEE Trans. Image Process. **27**, 5802–5812 (2018).
23. N. Banic and S. Loncaric, "Light random sprays Retinex: exploiting the noisy illumination estimation," IEEE Signal Process. Lett. **20**, 1240–1243 (2013).
24. N. Banic and S. Loncaric, "Smart light random memory sprays Retinex: a fast Retinex implementation for high-quality brightness adjustment and color correction," J. Opt. Soc. Am. A **32**, 2136–2147 (2015).
25. X. Ren, M. Li, W.-H. Cheng, and J. Liu, "Joint enhancement and denoising method via sequential decomposition," in *IEEE International Symposium on Circuits and Systems (ISCAS)* (IEEE, 2018), pp. 1–5.
26. W. Lu, T. Gao, C. Wang, B. Chen, and S. Zhang, "Low illumination color image enhancement algorithm based on fusion idea under retinex theory," Sci. Technol. Eng. **19**, 151–157 (2019).
27. Q. Zhang, Y. Nie, and W.-S. Zheng, "Dual illumination estimation for robust exposure correction," Comput. Graph. Forum **38**, 243–252 (2019).
28. X. Ren, W. Yang, W.-H. Cheng, and J. Liu, "LR3M: Robust low-light enhancement via low-rank regularized retinex model," IEEE Trans. Image Process. **29**, 5862–5876 (2020).
29. F. Liu, L. Liu, T. Hou, and Y. Liu, "Night road image enhancement method based on optimized MSR," J. Jilin Univ.- Eng. Technol. Ed. **51**, 323–330 (2021).
30. K. Zuiderveld, "Contrast limited adaptive histogram equalization," in *Graphics Gems IV* (1994), pp. 474–485.
31. C. Wei, W. Wang, W. Yang, and J. Liu, "Deep retinex decomposition for low-light enhancement," arXiv, arXiv:1808.04560 (2018).
32. Y. Zhang, J. Zhang, and X. Guo, "Kindling the darkness: A practical low-light image enhancer," in *Proceedings of the 27th ACM International Conference on Multimedia* (2019), pp. 1632–1640.
33. C. Guo, C. Li, J. Guo, C. C. Loy, J. Hou, S. Kwong, and R. Cong, "Zero-reference deep curve estimation for low-light image enhancement," in *Proceedings of the IEEE/CVF Conference on Computer Vision and Pattern Recognition* (2020), pp. 1780–1789.
34. L.-W. Wang, Z.-S. Liu, W.-C. Siu, and D. P. K. Lun, "Lightening network for low-light image enhancement," IEEE Trans. Image Process. **29**, 7984–7996 (2020).
35. Y. Jiang, X. Gong, D. Liu, Y. Cheng, C. Fang, X. Shen, J. Yang, P. Zhou, and Z. Wang, "Enlightengan: Deep light enhancement without paired supervision," IEEE Trans. Image Process. **30**, 2340–2349 (2021).
36. X. Jiang, *Research on Nighttime Image Under Poor Lighting Conditions Enhancement Method* (Harbin Institute of Technology, 2020).
37. J. Zhang, P. Zhou, and M. Xue, "Low-light image enhancement based on directional total variation retinex," J. Comput. Aided Des. Comput. Graph. **30**, 1943–1953 (2018).
38. K. Wang and F. Huang, "Multi-scale retinex image enhancement in HSV space based on illumination compensation," Laser Optoelectron. Prog. **10**, 102–113 (2022).
39. K. He, J. Sun, and X. Tang, "Guided image filtering," in *European Conference on Computer Vision* (Springer, 2010), pp. 1–14.
40. M. Jiang, G. Sha, and N. Li, "Infrared and visible image fusion based on guided filtering and dual tree complex wavelet transform," Laser Optoelectron. Prog. **39**, 1–18 (2022).
41. H.-Y. Zhang, X.-Q. Wang, H.-Y. Wang, and L.-C. Cao, "Advanced retinex-net image enhancement method based on value component processing," Acta Phys. Sin. **71**, 110701 (2022).
42. J. Xiong, X. Feng, G. Geng, and M. Zhou, "Real color image enhanced and denoised by stationary wavelet transform," Comput. Sci. **36**, 254–257 (2009).
43. L. I. Rudin, S. Osher, and E. Fatemi, "Nonlinear total variation based noise removal algorithms," Physica D **60**, 259–268 (1992).
44. Q. Wang, *Research on Image Denoising Algorithm Based on Total Variation Model* (Xi'an University of Technology, 2020).
45. X. Wang, *Study of Image Denoising and Decomposition Model and Its Algorithm Based on TV and the Fractional Order Derivatives* (Shandong University of Science and Technology, 2019).
46. N. Ni and B. Sun, "Image denoising algorithm based on total variation," Math. Theory Appl. **37**, 32–37 (2017).
47. X. Long and G. He, "Image enhancement method based on multi-layer fusion and detail recovery," Appl. Res. Comput. **37**, 584–587 (2020).
48. C. Zhang, B. Kang, Y. Li, and Y. Chang, "Underwater image enhancement based on differential channel gain and improved retinex," Laser Optoelectron. Prog. **58**, 156–163 (2021).
49. X. Guo, Y. Li, and H. Ling, "LIME: Low-light image enhancement via illumination map estimation," IEEE Trans. Image Process. **26**, 982–993 (2016).
50. S. Wang, J. Zheng, H.-M. Hu, and B. Li, "Naturalness preserved enhancement algorithm for non-uniform illumination images," IEEE Trans. Image Process. **22**, 3538–3548 (2013).